

# Thermal and velocity slip effects on the MHD peristaltic flow with carbon nanotubes in an asymmetric channel: application of radiation therapy

Noreen Sher Akbar · S. Nadeem · Zafar Hayat Khan

Received: 9 July 2013 / Accepted: 20 August 2013 / Published online: 13 September 2013  
© The Author(s) 2013. This article is published with open access at Springerlink.com

**Abstract** Peristaltic flow is used to study the flow and heat transfer of carbon nanotubes in an asymmetric channel with thermal and velocity slip effects. Two types of carbon nanotubes, namely, single- and multi-wall carbon nanotubes are utilized to see the analysis with water as base fluids. Empirical correlations are used for the thermophysical properties of carbon nanotubes (CNTs) in terms of solid volume fraction of CNTs. The governing equations are simplified using long wavelength and low Reynolds number approximation. Exact solutions have been evaluated for velocity, pressure gradient, the solid volume fraction of CNTs and temperature profile. The effects of various flow parameters, i.e. Hatmann number  $M$ , the solid volume fraction of the nanoparticles  $\phi$ , Grashof number  $G$ , velocity slip parameter  $\beta$ , thermal slip parameter  $\gamma$  and Prandtl number  $P_r$  are presented graphically for both single- (SWCNT) and multi-wall carbon nanotubes (MWCNT).

**Keywords** Peristaltic flow · Thermal and velocity slip · Asymmetric channel · Carbon nanotubes · MHD · Application of radiation therapy

## Introduction

Recently, peristalsis has been charmed much consideration due to its significant manufacturing and therapeutic applications, like chyme drive in the intestine, crusade of eggs in the fallopian tube, transport of the sperm in cervical canal, conveyance of bile in the bile duct, transport of cilia, circulation of blood in small blood vessels and in the intra-uterine fluid flow within the uterine cavity. From the time when the first investigation of Latham (1966) was done to discuss the peristaltic mechanism, numerous conjectural and experimental studies have been performed to comprehend the peristaltic feat [see (Shapiro et al. 1969; Zien and Ostrach 1970; Lee and Fung 1971; Srivastava et al. 1983)]. Specifically, to designate peristaltic flow in a symmetric or axisymmetric channels and tubes containing Newtonian or non-Newtonian fluids, many models have been examined by Elshehawey and Mekheimer (1994), Ramachandra and Usha (1995), Mekheimer and Elmaboud (2008), Srinivas and Kothandapani (2009), Srinivas et al (2009) and Nadeem and Akbar (2012b).

The nanofluids are a innovative class of resolutions proposed by scattering nanometer-sized materials (nanoparticles, nanofibers, nanotubes, nanowires, nanorods, nanosheet, or droplets) in base fluids. Peristalsis in connection with nanofluids has application in biomedicines, i.e. cancer treatment radiation therapy, etc. Choi (1995) testified that an advanced technique for mending heat transfer is by using nanoscale particles in the base fluid. Further, Choi et al. (1995) showed that the accumulation of a small amount ( $<1\%$  by volume) of nanoparticles to conformist heat transfer fluids increased the thermal conductivity of the fluid up to about two times. After Choi's (1995) first experiment on nanofluid, this topic has become quite interesting to the readers and researchers, including

N. S. Akbar (✉)  
DBS&H, CEME, National University of Sciences  
and Technology, Islamabad, Pakistan  
e-mail: noreensher1@gmail.com; noreensher@yahoo.com

S. Nadeem  
Department of Mathematics, Quaid-i-Azam University,  
Islamabad 45320, Pakistan

Z. H. Khan  
School of Mathematical Sciences, Peking University,  
Beijing 100871, People's Republic of China

Buongiorno (2006), Khanafer et al (2003), Das et al. (2003), Nield and Kuznetsov (2009), Kuznetsov and Nield (2010), Nield and Kuznetsov (2011), Akbar et al (2012a, b) and Akbar and Nadeem (2011, 2012a).

They emphasis on Ag–water and Cu–water nanofluids, and the properties of the nanoparticles volume fraction on the flow and heat transfer distinctiveness below the possessions of current resistance and temperature reliant inner heat invention or consolidation. Heat and mass transport inspection for boundary layer stagnation point flow in excess of a stretching spread in a porous medium soaked by a nanofluid with internal heat generation/absorption and suction/blowing is explored by Hamad and Ferdows (2012a). Very recently in another article, Hamad and Ferdows (2012b) studied the boundary layer flow and heat transfer in a viscous fluid encompassing metallic nanoparticles over a nonlinear stretching sheet. According to Hamad and Ferdows (2012b) the significantly intensifying the thermal conductivity of fluids by buildup very small quantities of composed tinny or metallic oxide nanoparticles (Cu, CuO, Al<sub>2</sub>O<sub>3</sub>) to the fluid, or instead using nanotube deferrals skirmishes with the classical theories of approximating the effective thermal conductivity of suspensions.

Nanotubes are affiliates of the fullerene structural family. Their name arises from their long, resonating edifice with the ramparts formed by one-atom-thick sheets of carbon, called graphene. These sheets are rolled at specific and discrete (“chiral”) angles, and the combination of the rolling angle and radius decides the nanotube properties; for example, whether the individual nanotube shell is a metal or semiconductor. Nanotubes are categorized as single-walled nanotubes (SWNTs) and multi-walled nanotubes (MWNTs). A new model of effective thermal conductivity of carbon nanotubes (CNTs) is presented by Xue (2005). He showed that the theoretical results of the effective thermal conductivity of CNTs/oil and CNTs/decene suspensions presented by him are in good agreement with the experimental data. The influence of multi-walled carbon nanotubes on single-phase heat transfer and pressure drop characteristics in the transitional flow regime of smooth tubes is presented by Meyer et al (2013). According to them, the increase in viscosity was four times the increase in the thermal conductivity. The heat transfer and pressure drop of nanofluids containing carbon nanotubes in a horizontal circular tube are experimentally investigated by Wang et al (2013). Very recently, homogeneous flow model is used by Khan et al (2013) to study the flow and heat transfer of CNTs along a flat plate subjected to Navier slip and uniform heat flux boundary conditions. According to them, engine oil-based CNTs have higher heat transfer rates than water and kerosene-based CNTs.

In the present article, the authors discuss the peristaltic flow of carbon nanotubes in an asymmetric channel with MHD. To the author’s knowledge, this is the first paper on the peristaltic flow of CNTs in an asymmetric channel. Two types of carbon nanotubes, namely, single- (SWCNT) and multi-wall carbon nanotubes (MWCNT) are used with water as base fluid. The empirical correlations are used for the thermo-physical properties of CNTs in terms of the solid volume fraction of CNTs. The governing equations are simplified using long wavelength and low Reynolds number approximation. Exact solutions have been evaluated for velocity, pressure gradient, the solid volume fraction of the nanoparticles and temperature profile. The effects of various flow parameters, i.e. Hatmann number  $M$ , the solid volume fraction of the nanoparticles  $\phi$ , Grashof number  $G$  and Prandtl number  $P_r$ , are presented graphically for both SWCNT and MWCNT.

### Formulation of the problem

We present an incompressible peristaltic flow of carbon nanotubes in an asymmetric channel with channel girth  $d_1 + d_2$  with thermal and velocity slip effects. Sinusoidal wave propagate down the walls of the channel with constant speed  $c_1$ . Asymmetry in the channel flow is due to the phase difference:

$$\begin{aligned} Y = \bar{H}_1 &= d_1 + a_1 \cos \left[ \frac{2\pi}{\lambda} (\bar{X} - c_1 \bar{t}) \right], \\ Y = \bar{H}_2 &= -d_2 - b_1 \cos \left[ \frac{2\pi}{\lambda} (\bar{X} - c_1 \bar{t}) + \omega \right]. \end{aligned} \quad (1)$$

In the above equations,  $a_1$  and  $b_1$  denote the waves’ amplitudes,  $\lambda$  is the wave length,  $d_1 + d_2$  is the channel width,  $c_1$  is the wave speed,  $\bar{t}$  is the time,  $\bar{X}$  is the direction of wave propagation and  $\bar{Y}$  is perpendicular to  $\bar{X}$ . The expression for fixed and wave frames are related by the following relations

$$\bar{x} = \bar{X} - c_1 t, \quad y = \bar{Y}, \quad \bar{u} = \bar{U} - c_1, \quad \bar{v} = \bar{V}, \quad p(\bar{x}) = P(\bar{X}, t). \quad (2)$$

With the transformation given in Eq. (2), equations governing the flow and temperature in the presence of heat source or heat sink with viscous dissipation are (Hamad and Ferdows 2012a, b)

$$\frac{\partial \bar{u}}{\partial \bar{x}} + \frac{\partial \bar{v}}{\partial \bar{y}} = 0, \quad (3)$$

$$\begin{aligned} \bar{u} \frac{\partial \bar{u}}{\partial \bar{x}} + \bar{v} \frac{\partial \bar{u}}{\partial \bar{y}} &= -\frac{1}{\rho_{nf}} \frac{\partial P}{\partial \bar{x}} + \frac{\mu_{nf}}{\rho_{nf}} \frac{\partial^2 \bar{u}}{\partial \bar{y}^2} + \frac{\mu_{nf}}{\rho_{nf}} \frac{\partial^2 \bar{u}}{\partial \bar{x}^2} - \frac{\sigma B_o^2}{\rho_{nf}} (\bar{u} + c_1) \\ &+ \frac{\rho_{nf}}{\rho_{nf}} g \alpha (\bar{T} - \bar{T}_0), \end{aligned} \quad (4)$$

$$\bar{u} \frac{\partial \bar{v}}{\partial \bar{x}} + \bar{v} \frac{\partial \bar{v}}{\partial \bar{y}} = -\frac{1}{\rho_{nf}} \frac{\partial P}{\partial \bar{y}} + \frac{\mu_{nf}}{\rho_{nf}} \frac{\partial^2 \bar{v}}{\partial \bar{y}^2} + \frac{\mu_{nf}}{\rho_{nf}} \frac{\partial^2 \bar{v}}{\partial \bar{x}^2}, \quad (5)$$

$$\bar{u} \frac{\partial \bar{T}}{\partial \bar{x}} + \bar{v} \frac{\partial \bar{T}}{\partial \bar{y}} = \alpha_{nf} \left( \frac{\partial^2 \bar{T}}{\partial \bar{y}^2} + \frac{\partial^2 \bar{T}}{\partial \bar{x}^2} \right) + \frac{Q_0}{(\rho c_p)_{nf}}, \quad (6)$$

where  $\bar{x}$  and  $\bar{y}$  are the coordinates along and perpendicular to the channel,  $\bar{u}$  and  $\bar{v}$  are the velocity components in the  $\bar{x}$  and  $\bar{y}$  directions, respectively, and  $\bar{T}$  is the local temperature of the fluid. Further,  $\rho_{nf}$  is the effective density,  $\mu_{nf}$  the effective dynamic viscosity,  $(\rho c_p)_{nf}$  the heat capacitance,  $\alpha_{nf}$  the effective thermal diffusivity,  $k_{nf}$  the effective thermal conductivity of the nanofluid and  $Q_0$  is constant heat absorption parameter which are defined as [see (Xue 2005; Wang et al. 2013)]

$$\begin{aligned} \rho_{nf} &= (1 - \phi) \rho_f + \phi \rho_f, \mu_{nf} = \frac{\mu_f}{(1 - \phi)^{2.5}}, \\ (\rho c_p)_{nf} &= (1 - \phi) (\rho c_p)_f + \phi (\rho c_p)_s, \alpha_{nf} = \frac{k_{nf}}{(\rho c_p)_{nf}}, \\ \frac{k_{nf}}{k_f} &= \frac{(1 - \phi) + 2\phi \frac{k_{CNT}}{k_{CNT} - k_f} \ln \frac{k_{CNT} + k_f}{2k_f}}{(1 - \phi) + 2\phi \frac{k_f}{k_{CNT} - k_f} \ln \frac{k_{CNT} + k_f}{2k_f}} \end{aligned} \quad (7)$$

where  $\phi$  is the solid volume fraction of the CNTs.

We introduce the following non-dimensional quantities

$$\begin{aligned} x &= \frac{2\pi \bar{x}}{\lambda}, y = \frac{\bar{y}}{d_1}, u = \frac{\bar{u}}{c_1}, v = \frac{\bar{v}}{c_1}, t = \frac{2\pi \bar{t}}{\lambda}, \delta = \frac{2\pi d_1}{\lambda}, \\ &= \frac{d_2}{d_1}, P = \frac{2\pi d_1^2 P}{\mu_f c_1 \lambda}, \\ h_1 &= \frac{\bar{h}_1}{d_1}, h_2 = \frac{\bar{h}_2}{d_2}, \text{Re} = \frac{\rho c_1 d_1}{\mu_f}, a = \frac{a_1}{d_1}, b = \frac{a_2}{d_1}, d = \frac{d_2}{d_1}, \\ S &= \frac{\bar{S} d_1}{\mu_f c_1} \\ \theta &= \frac{\bar{T} - \bar{T}_0}{\bar{T}_1 - \bar{T}_0}, P_r = \frac{v}{\alpha}, \beta_1 = \frac{Q_0 d_1^2}{(\bar{T}_1 - \bar{T}_0) k_f}, M^2 = \frac{\sigma B_0^2 d_1^2}{\mu_f}, \\ G_r &= \frac{g \alpha d_1^2 (\bar{T}_1 - \bar{T}_0)}{v c_1}. \end{aligned} \quad (8)$$

In the above equations  $P_r$  is the Prandtl number and  $E_c$  is the Eckert number.

Stream function and velocity field are related by the expressions

$$u = \frac{\partial \Psi}{\partial y}, v = -\delta \frac{\partial \Psi}{\partial x}. \quad (9)$$

In view of Eqs. (7–9) under the the long wavelength and low Reynolds number assumption, we have the following equations

$$\frac{1}{(1 - \phi)^{2.5}} \frac{\partial^4 \Psi}{\partial y^4} - M^2 \frac{\partial^2 \Psi}{\partial y^2} + G_r \frac{\partial \theta}{\partial y} = 0, \quad (10)$$

$$\frac{dP}{dx} = \frac{\partial}{\partial y} \left[ \frac{1}{(1 - \phi)^{2.5}} \frac{\partial^2 \Psi}{\partial y^2} - M^2 \left( \frac{\partial \Psi}{\partial y} + 1 \right) \right] + G_r \theta, \quad (11)$$

$$\frac{\partial^2 \theta}{\partial y^2} + \left( \frac{(1 - \phi) + 2\phi \frac{k_f}{k_{CNT} - k_f} \ln \frac{k_{CNT} + k_f}{2k_f}}{(1 - \phi) + 2\phi \frac{k_{CNT}}{k_{CNT} - k_f} \ln \frac{k_{CNT} + k_f}{2k_f}} \right) \beta_1 = 0. \quad (12)$$

The non-dimensional boundary conditions are

$$\Psi = \frac{F}{2}, \frac{\partial \Psi}{\partial y} = -\beta \frac{\partial^2 \Psi}{\partial y^2} - 1, \quad \text{at } y = h_1 = 1 + a \cos x, \quad (12a)$$

$$\Psi = -\frac{F}{2}, \frac{\partial \Psi}{\partial y} = \beta \frac{\partial^2 \Psi}{\partial y^2} - 1, \quad \text{at } y = h_2 = -d - b \cos(x + \phi), \quad (12b)$$

$$\theta + \gamma \frac{\partial \theta}{\partial y} = 0, \quad \text{at } y = h_1, \theta - \gamma \frac{\partial \theta}{\partial y} = 1 \text{ at } y = h_2. \quad (12c)$$

The flow rates in fixed and wave frame are related by

$$Q = F + 1 + d. \quad (13)$$

## Solution profiles

The exact solutions for stream function, solid volume fraction of the nanoparticles and pressure gradient can be written as

$$\begin{aligned} \Psi(x, y) &= G_r (1 - \phi)^{2.5} y^2 (6 + (h_1 - h_2) \\ &\quad \times \frac{(1 - \phi) + 2\phi \frac{k_{CNT}}{k_{CNT} - k_f} \ln \frac{k_{CNT} + k_f}{2k_f}}{(1 - \phi) + 2\phi \frac{k_f}{k_{CNT} - k_f} \ln \frac{k_{CNT} + k_f}{2k_f}} \\ &\quad \times (3(h_1 + h_2) - 2y) \beta_1) + 12(h_1 - h_2) M^2 \\ &\quad \times (1 - \phi)^{2.5} (L_{15} + y L_{16}) + 12(h_1 - h_2) \\ &\quad \times (L_{13} + L_{14}) \cosh(My(1 - \phi)^{\frac{5}{2}}) \\ &\quad + (L_{13} - L_{14}) \sinh(My(1 - \phi)^{\frac{5}{2}}) \\ &\quad / (12(h_1 - h_2) M^2 (1 - \phi)^{2.5}), \end{aligned} \quad (14)$$

$$\begin{aligned} \frac{dP}{dx} &= L_{12} (L_2 - L_5) (1 + L_7) - L_{12} (F - L_1 + L_4) L_8 \\ &\quad + (L_3 - L_6) (L_{11} (1 + L_7) - (1 + L_{10}) L_8) \\ &\quad + (L_{11} (F - L_1 + L_4) + (1 + L_{10}) (L_2 - L_5)) \\ &\quad \times L_9 / (L_3 - L_6) (L_{11} - L_8) + L_{12} (L_2 - L_5 - h_1 \\ &\quad \times L_8 + h_2 L_8) + (h_1 L_{11} - h_2 L_{11} - L_2 + L_5) L_9 \end{aligned} \quad (15)$$

$$\theta(x, y) = 1/2 \left( 1 + \left( \frac{(1 - \phi) + 2\phi \frac{k_{CNT}}{k_f} \ln \frac{k_{CNT} + k_f}{2k_f}}{(1 - \phi) + 2\phi \frac{k_f}{k_{CNT} - k_f} \ln \frac{k_{CNT} + k_f}{2k_f}} \right) \times (h_1 - y)(-h_2 + y)\beta_1 + (h_1 - h_2) \times \left( \frac{(1 - \phi) + 2\phi \frac{k_{CNT}}{k_f} \ln \frac{k_{CNT} + k_f}{2k_f}}{(1 - \phi) + 2\phi \frac{k_f}{k_{CNT} - k_f} \ln \frac{k_{CNT} + k_f}{2k_f}} \right) \beta_1 \gamma \times \frac{h_1 + h_2 - 2\gamma}{h_1 - h_2 + 2\gamma} \right). \quad (16)$$

where  $L_1 - L_{16}$  are constants evaluated using Mathematica 8.

The dimensionless pressure rise  $\Delta P$  is

$$\Delta P = \int_0^1 \left( \frac{dP}{dx} \right) dx. \quad (17)$$

## Graphical illustration

To see the significance of CNTs graphically and physically for the pressure rise, pressure gradient, velocity, temperature profile, solid volume fraction of the CNTs and streamlines for the flow parameter for the numerical values are plotted in Figs. 1, 2, 3, 4, and 5. Analysis have been done for Cu nanoparticles with water as a base fluid in connection with SWCNT and MWCNT with the application of thermal and velocity slip effects. Numerical integration is performed for the pressure rise per wavelength. The pressure rise against volume flow rate for the solid volume fraction of the nanoparticles  $\phi$ , Hartmann number  $M$ , slip parameter  $\beta$ , and Grashof number  $G_r$  is depicted in Fig. 1a–d. It is noticed that the pressure rise and volume flow rate have opposite behaviours. From Fig. 1a–d it is seen that in the pumping

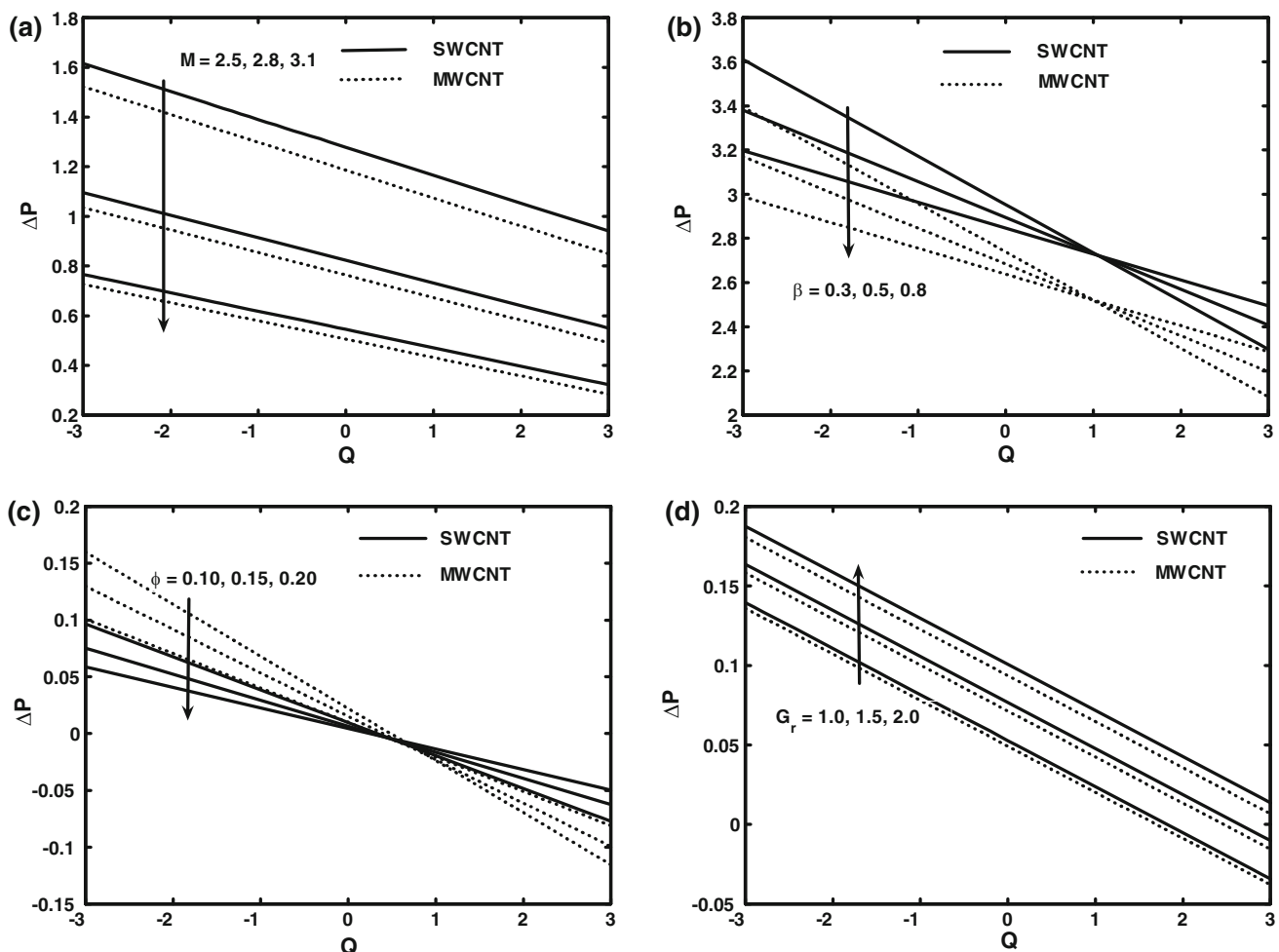


**Fig. 1** Pressure rise versus flow rate **a**  $\beta = 0.5$ ,  $\phi = 0.2$ ,  $G_r = 2$ . **b**  $M = 2$ ,  $\phi = 0.2$ ,  $G_r = 2$ . **c**  $M = 4$ ,  $\beta = 0.5$ ,  $G_r = 2$ , and **d**  $\beta = 0.5$ ,  $\phi = 0.2$ ,  $M = 2$ . Other parameters are  $a = 0.2$ ,  $b = 0.2$ ,  $d = 1$ ,  $\beta_1 = 0.2$ ,  $\gamma = 0.2$

region ( $\Delta P > 0$ ), the pressure rise decreases with the increase of Hartman number  $M$ , while pressure rise increases with the increase in the Hartmann number  $M$ , solid volume fraction of the CNTs  $\phi$  and slip parameter  $\beta$  and pressure rise increases by increasing Grashof number  $G_r$ . Figure 1a, d also shows that in the augmented pumping region for ( $\Delta P < 0$ ), pressure rise gives the opposite results for all the parameters as compared to the pumping region ( $\Delta P > 0$ ). Free pumping region holds when ( $\Delta P = 0$ ). It is also seen that the pressure rise for SWCNTs is greater as compared to the MWCNT. Variations of Hartmann number  $M$ , solid volume fraction  $\phi$  of the CNTs, Hartmann number  $M$  and slip parameter  $\beta$  on the velocity profile are shown in Fig. 2a–d. It depicts that the behaviour of velocity is not similar in view of the Hartmann number  $M$ , solid volume fraction  $\phi$  of the CNTs, Hartmann number  $M$  and slip parameter  $\beta$ . The velocity field increases due to increase

**Table 1** Thermal properties of base fluid (water) and nanoparticles

Physical properties	Fluid Phase (Water)	SWCNT	MWCNT
$c_p$ (J/kg K)	4,179	425	796
$\rho$ (kg/m <sup>3</sup> )	997.1	2,600	1,600
$k$ (W/mk)	0.613	6,600	3,000

in  $\phi$ ,  $\beta$ , and  $G_r$  at the centre of the channel, while velocity field decreases with an increase in  $\phi$ ,  $\beta$ , and  $G_r$  near the channel wall. It is also analyzed that the velocity field decreases due to increase in  $M$  at the centre of the channel, while velocity field increases with an increase in  $M$  near the channel wall. It is also observed that the velocity field for SWCNT is greater than that compared to the MWCNT in view of  $M$  and  $\phi$ , while the velocity field for SWCNT is greater than that compared to the MWCNT in view of  $\beta$  and  $G_r$  (Table 1).

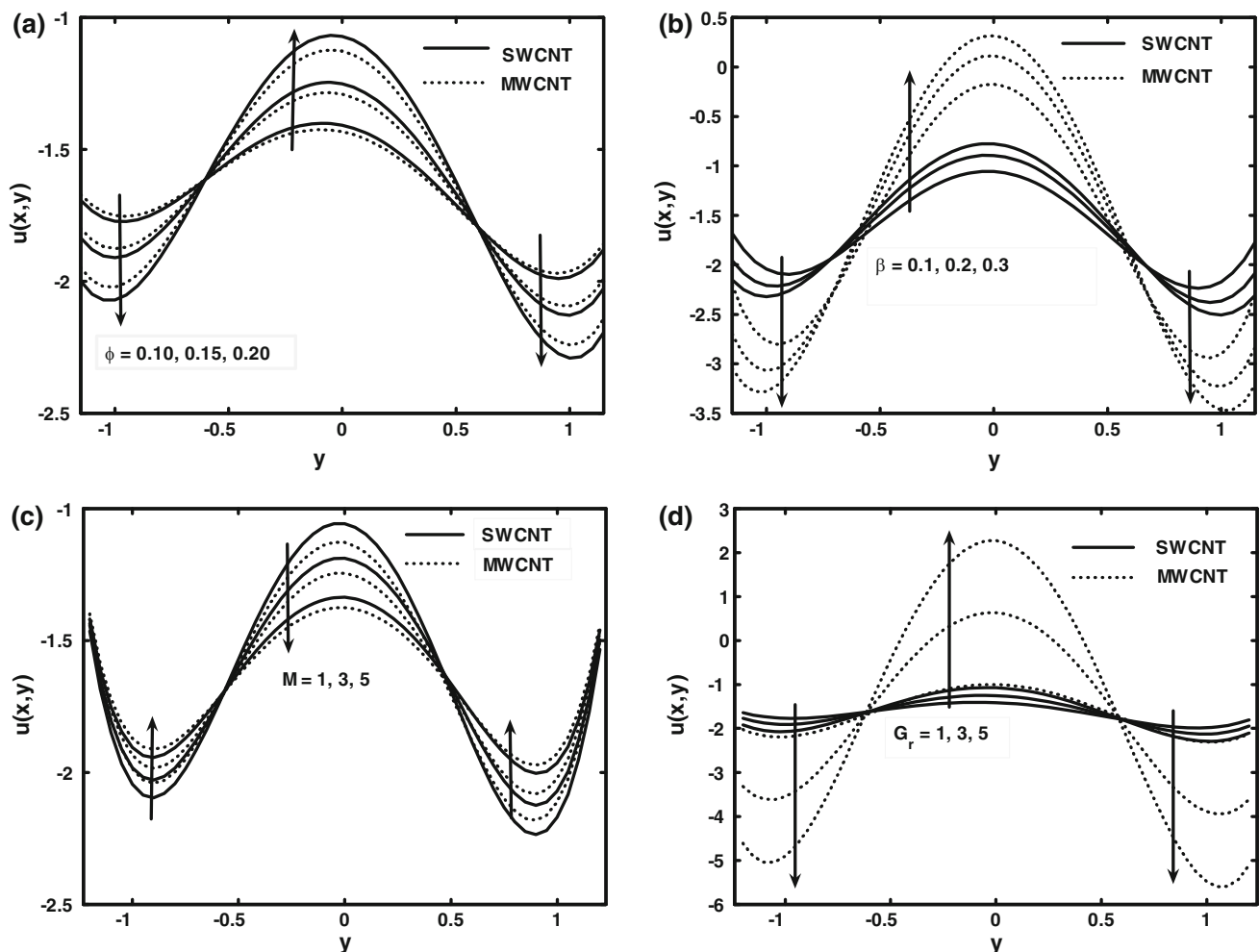


**Fig. 2** Velocity profile **a**  $\beta = 0.5, M = 2, G_r = 2$ , **b**  $M = 2, \phi = 0.2, G_r = 2$ , **c**  $\phi = 0.2, \beta = 0.5, G_r = 2$ , and **d**  $\beta = 0.5, \phi = 0.2, M = 2$ . Other parameters are  $a = 0.2, b = 0.2, d = 1, \beta_1 = 0.2, \gamma = 0.2$

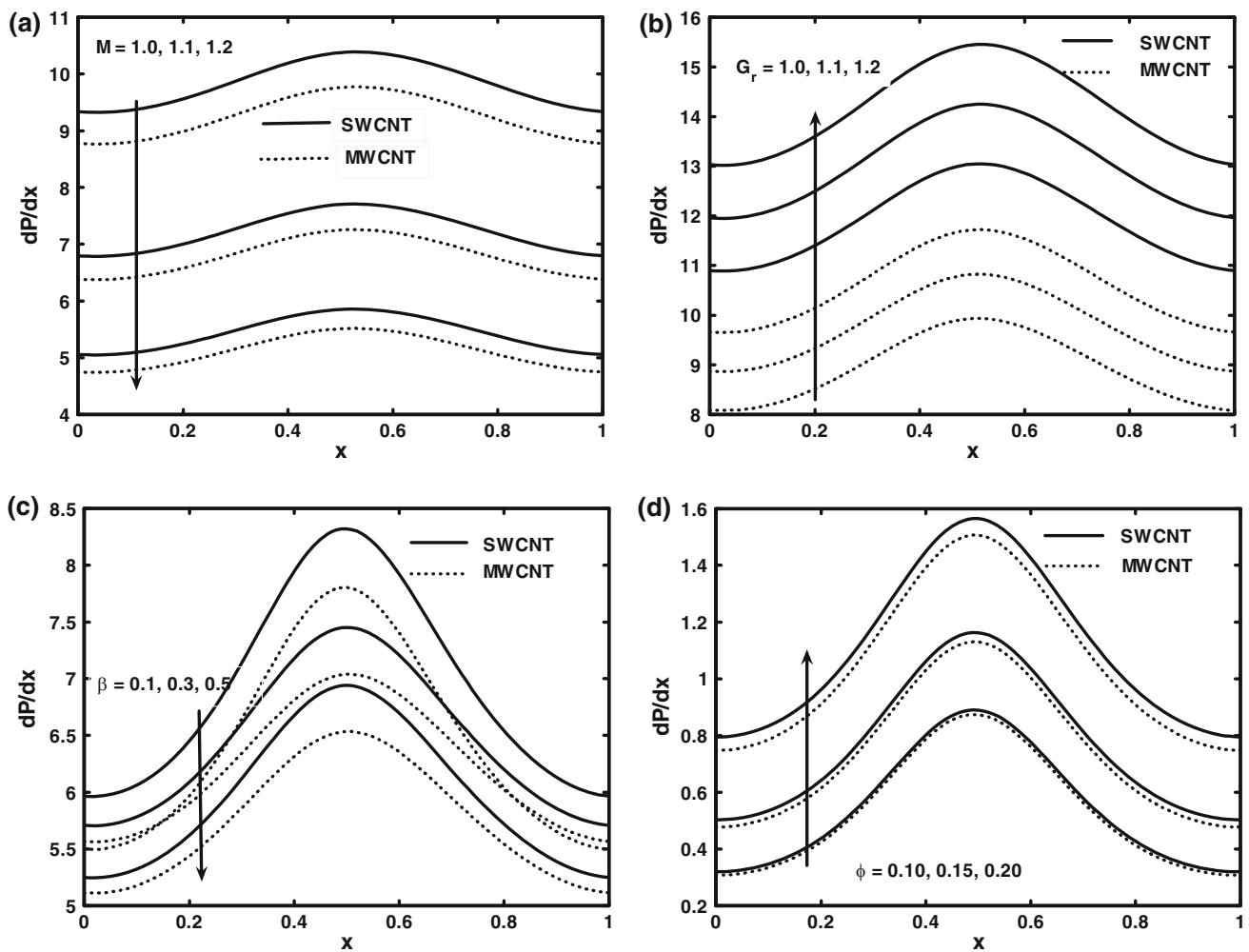


**Fig. 3** Pressure gradient **a**  $\beta = 0.5$ ,  $\phi = 0.2$ ,  $G_r = 2$ , **b**  $M = 2$ ,  $\phi = 0.2$ ,  $\beta = 0.2$ , **c**  $\phi = 0.2$ ,  $M = 2$ ,  $G_r = 2$ , and **d**  $\beta = 0.5$ ,  $G_r = 2$ ,  $M = 2$ . Other parameters are  $a = 0.2$ ,  $b = 0.2$ ,  $d = 1$ ,  $\beta_1 = 0.2$ ,  $\gamma = 0.2$

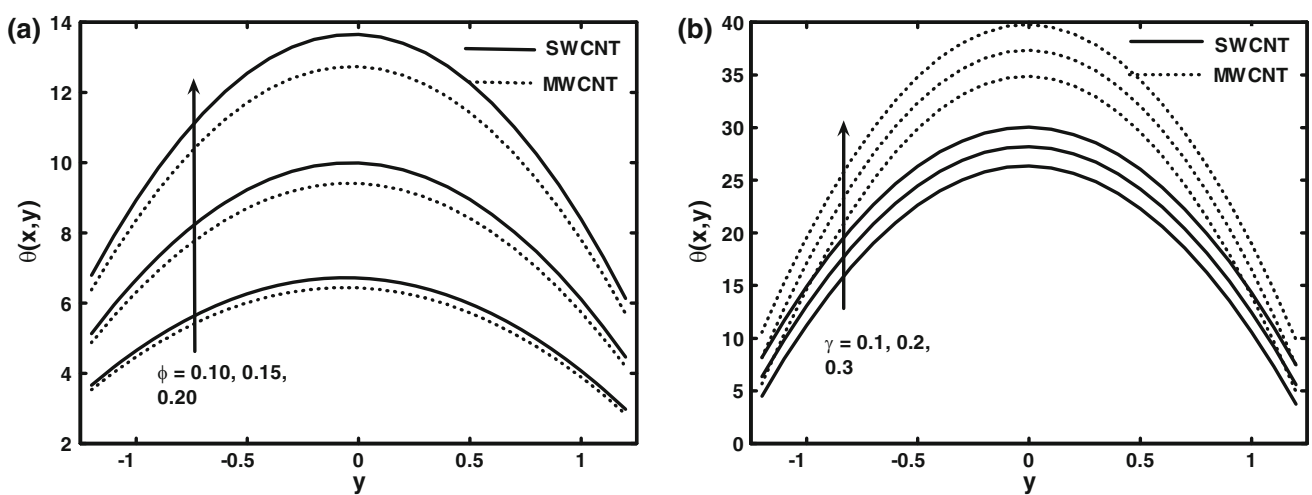


**Fig. 4** Temperature profile **a**  $\gamma = 0.2$ , **b**  $\phi = 0.2$ . The other parameters are  $a = 0.2$ ,  $b = 0.2$ ,  $d = 1$ ,  $\beta_1 = 0.2$



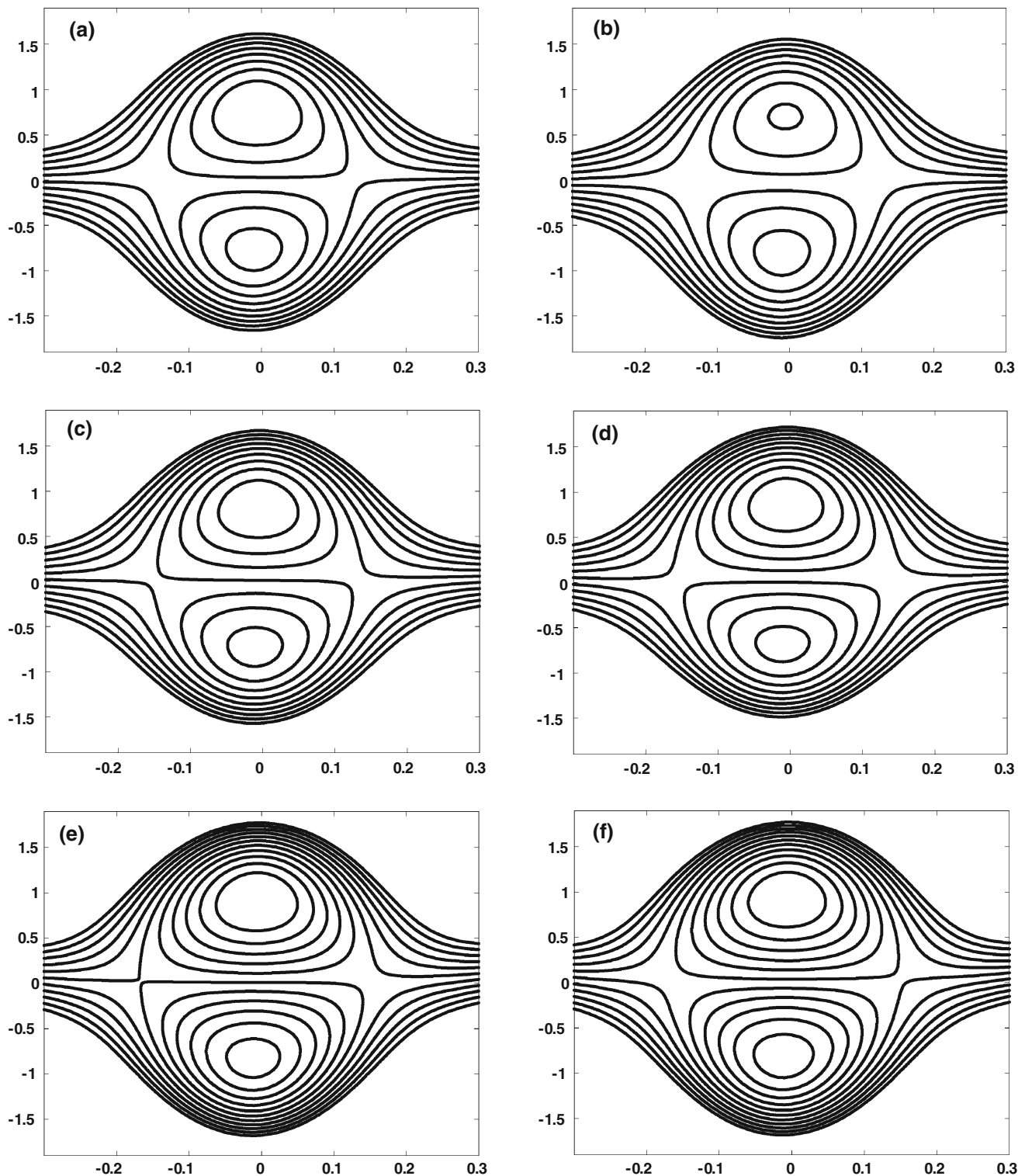


**Fig. 5** Streamlines for **a, b** SWCNT and MWCNT, **c, d** for  $\phi = 0.3, 0.4$ , with SWCNT, **e, f** for  $\phi = 0.3, 0.4$ , with MWCNT; other parameters are  $\beta = 0.3, d = 1, \omega = 0.3, b = 0.4, a = 0.2, Q = -2$

The pressure gradient for different values of  $M, G_r, \beta$  and  $\phi$  are plotted in Fig. 3a–d. The magnitude of pressure gradient increases with the increase in  $G_r$ , and  $\phi$ . It is also observed that the maximum pressure

gradient occurs when  $x = 0.48$  and near the channel walls the pressure gradient is small. This leads to the fact that flow can easily pass at the middle of the channel. It is analyzed that the pressure gradient

decreases with an increase in  $M$  and  $\beta$ . It is also observed that the pressure gradient for MWCNT is greater than that compared to SWCNT.

Variations of temperature profile for different values of thermal slip parameter  $\gamma$  and solid volume fraction of the CNTs  $\phi$  can be seen in Fig. 4a, b. It is analyzed that when we increase slip parameter  $\gamma$  and solid volume fraction of the CNTs  $\phi$  the temperature profile increases. It is also seen that temperature for MWCNT is greater than that compared to SWCNT with varying values of  $\phi$  and  $\gamma$ .

The trapping for different values of solid volume fraction of the CNTs with SWCNT and MWCNT is shown in Fig. 5a–d. It is seen from Fig. 5a, b that the size and number of the trapping bolus decreases for MWCNT as compared to SWCNT. Streamlines for different values of  $\phi$  for SWCNT have been plotted in the Fig. 5c, d. It is found that when we increase  $\phi$  for SWCNT, the number of trapping bolus increases, but the size of trapped bolus decreases. Streamlines for different values of  $\phi$  for MWCNT have been plotted in Fig. 5e, f. It is found that when we increase  $\phi$  for SWCNT, the size of the trapped bolus decreases; the number of trapping bolus increases when we increase  $\phi$  for MWCNT.

## Conclusions

The peristaltic flow of an incompressible carbon nanotubes in an asymmetric channel with thermal and velocity slip is discussed. This is the first paper on the peristaltic flow with the influence of CNTs in an asymmetric channel with slip effects.

- It is noticed that the pressure rise and volume flow rate have opposite behaviours.
- It is seen that pressure rise increases with the increase in the Hartmann number  $M$ , solid volume fraction of the CNTs  $\phi$  and slip parameter  $\beta$ ; pressure rise increases by increasing Grashof number  $G_r$ .
- It is also seen that pressure rise for SWCNTs is greater as compared to MWCNT.
- The velocity field increases due to increase in  $\phi$ ,  $\beta$  and  $G_r$  at the centre of the channel, while the velocity field decreases with an increase in  $\phi$ ,  $\beta$  and  $G_r$  near the channel wall.
- It is also observed that velocity field for SWCNT is greater than that compared to MWCNT in view of  $M$  and  $\phi$ .
- The magnitude of pressure gradient increases with the increase in  $G_r$  and  $\phi$ .
- It is analyzed that when we increase slip parameter  $\gamma$  and solid volume fraction of the CNTs  $\phi$ .

- It is found that when we increase  $\phi$  for SWCNT, the number of the trapping bolus increases, but the size of the trapped bolus decreases.

**Open Access** This article is distributed under the terms of the Creative Commons Attribution License which permits any use, distribution, and reproduction in any medium, provided the original author(s) and the source are credited.

## References

- Akbar NS, Nadeem S (2011) Endoscopic effects on the peristaltic flow of a nanofluid. *Commun Theor Phys* 56:761–768
- Akbar NS, Nadeem S (2012a) Peristaltic flow of a Phan-Thien-Tanner nanofluid in a diverging tube. *Heat Transf Asian Res* 41:10–22
- Akbar NS, Nadeem S (2012b) Thermal and velocity slip effects on the peristaltic flow of a six constant Jeffrey's fluid model. *Int J Heat Mass Transf* 55:3964–3970
- Akbar NS, Nadeem S, Hayat T, Hendi AA (2012a) Peristaltic flow of a nanofluid with slip effects. *Meccanica* 47:1283–1294
- Akbar NS, Nadeem S, Hayat T, Hendi AA (2012b) Peristaltic flow of a nanofluid in a non-uniform tube. *Heat Mass Transf* 48:451–459
- Buongiorno J (2006) Convective transport in nanofluids. *ASME J Heat Transf* 128:240–250
- Choi SUS (1995) Enhancing thermal conductivity of fluids with nanoparticles. In: Siginer DA, Wang HP (eds) *Developments and applications of non-Newtonian flows*, vol 66. ASME, New York, pp 99–105
- Das SK, Putra N, Roetzel W (2003) Pool boiling of nano-fluids on horizontal narrow tubes. *Int. J Multiph Flow* 29:1237–1247
- Elshehawey EF, Mekheimer KhS (1994) Couple-stresses in peristaltic transport of fluids. *J Phys D Appl Phys* 27:1163–1170
- Hamad MAA, Ferdows M (2012a) Similarity solution of boundary layer stagnation-point flow towards a heated porous stretching sheet saturated with a nanofluid with heat absorption/generation and suction/blowing: a Lie group analysis. *Commun Nonlinear Sci Numer Simul* 17:132–140
- Hamad MAA, Ferdows M (2012b) Similarity solutions to viscous flow and heat transfer of nanofluid over nonlinearly stretching sheet. *Appl Math Mech Engl Ed* 33(7):923–930
- Khan WA, Khan ZH, Rahi M (2013) Fluid flow and heat transfer of carbon nanotubes along a flat plate with Navier slip boundary. *Appl Nanosci*. doi:10.1007/s13204-013-0242-9
- Khanfer K, Vafai K, Lightstone M (2003) Buoyancy-driven heat transfer enhancement in a two-dimensional enclosure utilizing nanofluids. *Int J Heat Mass Transf* 46:3639–3653
- Kuznetsov AV, Nield DA (2010) Natural convective boundary-layer flow of a nanofluid past a vertical plate. *Int J Therm Sci* 49:243–247
- Latham TW (1966) Fluid motion in a peristaltic pump. MS. Thesis, Massachusetts Institute of Technology, Cambridge
- Lee JS, Fung YC (1971) Flow in non-uniform small blood vessels. *Microvasc Res* 3:272–287
- Mekheimer KhS, Abd Elmaboud Y (2008) The influence of heat transfer and magnetic field on peristaltic transport of a Newtonian fluid in a vertical annulus: application of an endoscope. *Phys Lett A* 372:1657–1665
- Meyer J, McKrell T, Grote K (2013) The influence of multi-walled carbon nanotubes on single-phase heat transfer and pressure drop characteristics in the transitional flow regime of smooth tubes. *Int J Heat Mass Transf* 58:597–609



- Nield DA, Kuznetsov AV (2009) The Cheng–Minkowycz problem for natural convective boundary-layer flow in a porous medium saturated by a nanofluid. *Int J Heat Mass Transf* 52:5792–5795
- Nield DA, Kuznetsov AV (2011) The Cheng–Minkowycz problem for the double-diffusive natural convective boundary layer flow in a porous medium saturated by a nanofluid. *Int J Heat Mass Transf* 54:374–378
- Ramachandra RA, Usha S (1995) Peristaltic transport of two immiscible viscous fluids in a circular tube. *J Fluid Mech* 298:271–285
- Shapiro AH, Jaffrin MY, Weinberg SL (1969) Peristaltic pumping with long wavelengths at low Reynolds number. *J Fluid Mech* 37:799–825
- Srivastava LM, Srivastava VP, Sinha SN (1983) Peristaltic transport of a physiological fluid: Part I. Flow in non-uniform geometry. *Biorheology* 20:153–166
- Srinivas S, Kothandapani M (2009) The influence of heat and mass transfer on MHD peristaltic flow through a porous space with compliant walls. *Appl Math Comput* 213:197–208
- Srinivas S, Gayathri R, Kothandapani M (2009) The influence of slip conditions, wall properties and heat transfer on MHD peristaltic transport. *Comput. Phys Commun* 180:2115–2122
- Wang J, Zhu J, Zhang X, Chen Y (2013) Heat transfer and pressure drop of nanofluids containing carbon nanotubes in laminar flows. *Exp Therm Fluid Sci* 44:716–721
- Xue Q (2005) Model for thermal conductivity of carbon nanotube-based composites. *Phys B Condens Matter* 368:302–307
- Zien TF, Ostrach SA (1970) A long wave approximation to peristaltic motion. *J Biomech* 3:63–75